Open Access

Nicole Hadert*, Qi Liu and Waldemar Zylka

Numerical examinations of simplified spondylodesis models concerning energy absorption in magnetic resonance imaging

DOI 10.1515/cdbme-2016-0143

Abstract: Metallic implants in magnetic resonance imaging (MRI) are a potential safety risk since the energy absorption may increase temperature of the surrounding tissue. The temperature rise is highly dependent on implant size. Numerical examinations can be used to calculate the energy absorption in terms of the specific absorption rate (SAR) induced by MRI on orthopaedic implants. This research presents the impact of titanium osteosynthesis spine implants, called spondylodesis, deduced by numerical examinations of energy absorption in simplified spondylodesis models placed in 1.5 T and 3.0 T MRI body coils. The implants are modelled along with a spine model consisting of vertebrae and disci intervertebrales thus extending previous investigations [1, 2]. Increased SAR values are observed at the ends of long implants, while at the center SAR is significantly lower. Sufficiently short implants show increased SAR along the complete length of the implant. A careful data analysis reveals that the particular anatomy, i.e. vertebrae and disci intervertebrales, has a significant effect on SAR. On top of SAR profile due to the implant length, considerable SAR variations at small scale are observed, e.g. SAR values at vertebra are higher than at disc positions.

Keywords: SAR; MRI; osteosynthesis implants; numerical simulation.

1 Introduction

MRI is considered as a secure imaging method in medical diagnosis [3]. However the electromagnetic fields might

*Corresponding author: Nicole Hadert, Faculty of Electrical Engineering and Applied Natural Sciences, Westphalian University Campus Gelsenkirchen, Germany, E-mail: n.h87@gmx.net Qi Liu: School of Engineering, Physics and Mathematics, University of Dundee, Dundee, UK

Waldemar Zylka: Faculty of Electrical Engineering and Applied Natural Sciences, Westphalian University Campus Gelsenkirchen, Germany, E-mail: waldemar.zylka@w-hs.de

be safety hazards for the human body. Particularly the energy of the high frequency field B_1 might by absorbed by metallic structures like implants. The absorbed energy is converted to heat resulting in potential temperature increase of tissue [4]. In medical application the body tissue temperature should not increase more than 1°C. It approximately corresponds to SAR = 4 W/kg in whole body or, dependent on region, SAR = 4–10 W/kg dependent on the body weight. Temperature of 43°C or more causes tissue injury [4, 5]. MRI examinations on patients with metallic implants are at discretion of medical professions and associated with individual risk.

Numerical modelling and simulation is a technique to access the impact of B_1 field on SAR and temperature. Only very few studies investigate numerical modelling of orthopedic implants. For an implant consisting of a rod with pins at its ends and placed in aqueous gel increasing SAR is observed at the ends of a conductive bar [1]. For external fixation device SAR depends on pin spacing and insertion depth (into the gel) [2]. In both studies spine is not modeled. This research focuses on the calculation of energy absorption of different simplified models of spondylodesis exposed to B_1 field. Spondylodesis is an implant where concerned spine segments are fixed with screw-rod-system. Thus, all models explicitly include vertebrae and disci intervertebrales.

2 Methods

Numerical examinations of energy absorption via MRI simulations are executed with the software Electromagnetic Suite 15 from ANSYS, Inc. Various models of MRI body coils, spine and spondylodesis implants have been developed and examined for 1.5 T/64 MHz and 3 T/128 MHz.

2.1 MRI coil models and SAR

The high frequency field of the MRI body coil model for 1.5 T MRI calculations is generated by a quadrature

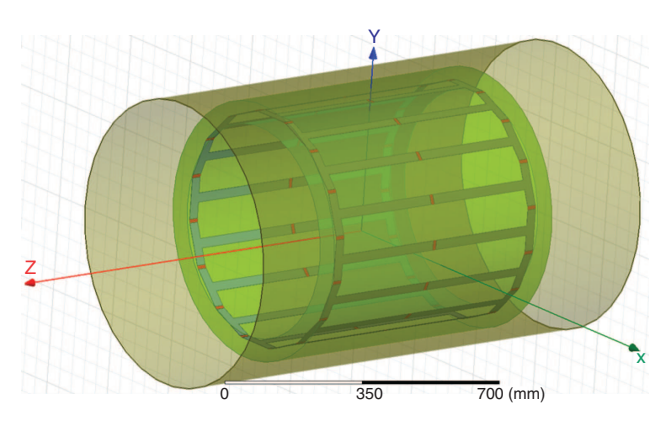


Figure 1: Model of MRI body coil with RF shield.

birdcage coil [6]. The high frequency field for the 3 T MRI simulations is generated by a model of a multi-transmit coil. It divides the B_1 field into separate B_1 subfields by using the ports as independent power supply channels. The induced electrical field is $E_{max}=90$ V/m. Both body coils (1.5 T and 3 T) are cylinders with height h=650 mm and diameter d=620 mm (Figure 1). Inside the quadrature coil an almost homogeneous magnetic field $B_1=1.4~\mu T$ is generated. Inside the multi-transmit coil an almost homogeneous magnetic field $B_1=1.5~\mu T$ is generated.

Electromagnetic fields are calculated by solving Maxwell equations. For SAR calculation first the particular tissue densities and local SAR in finite elements must be determined. Then the SAR algorithm runs on voxels, which are generated from finite elements [8]. Local SAR is defined as the dissipated power P_{diss} per mass m at the point r. It depends on intensity of the induced electrical field E and specific electrical conductivity σ of tissue and its density ρ .

$$SAR(\mathbf{r}) = \frac{1}{V} \int_{V} \frac{P_{diss}}{m} dV = \frac{1}{V} \int_{V} \frac{\sigma(\mathbf{r})}{2\rho(\mathbf{r})} |\mathbf{E}(\mathbf{r})|^{2} dV$$

It is specified by international safety norm IEC 606012-33 [9]. Here we use m = 10 g. Along with the tissue density this mass defines a volume V around this tissue point. Specific physical and electrical parameters, mass density, conductivity, permittivity, and permeability of each tissue or material of the model has to be set. Values can be found in literature, e.g. [10, 11].

2.2 Spondylodesis models

The torso phantom is a plexiglas body filled with liquid. The electromagnetic parameters of liquid are similar to those of tissue [6]. Its electrical conductivity is

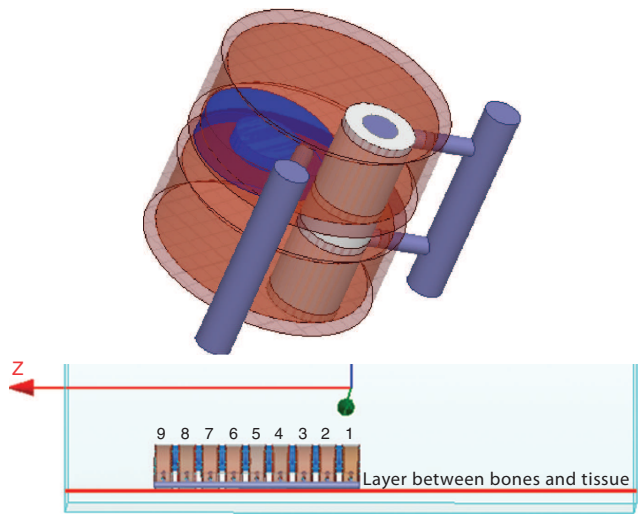


Figure 2: Top: Simplified spondylodesis model, the description is given in the main text. Bottom: Part of torso phantom with imbedded large spondylodesis over nine vertebrae, positions of vertebrae in Table 1. The red line indicates layer where SAR profiles are examined.

Table 1: Positions of vertebrae in torso phantom.

Model	Position [mm]		
	Distal	Proximal	
2 vertebrae	141.7-151.7	155–165	
9 vertebrae	48.6-58.6	155–165	

 $\sigma = 0.47 \; (\Omega \text{m})^{-1}$ and relative permittivity $\epsilon_r = 81 \; \text{F/m}$. The torso phantom is placed in the body coil in order to represent a human torso lying on his back in the MRI.

Simplified models for multi-vertebrae sections of spine are developed and combined with a simplified model of osteosynthesis spine implants:

- a two vertebrae model and a nine vertebrae model concentrated on the ventral static support motion elements of spine
- 2. a small spondylodesis over two vertebrae and a large spondylodesis over nine vertebrae
- 3. additionally two vertebrae positioned at both edges of the spondylodesis models (only for 1.5 T MRI)

The simplified spondylodesis model concentrates on the ventral static support of the movement elements of spine. The blue discs represent disci intervertebrales, the whitegrey cylinder medulla spinalis, the brown cylinders corpus vertebrae and foramen vertebrae and the grey rods represent screws and frame rods of the implant (Figure 2). The

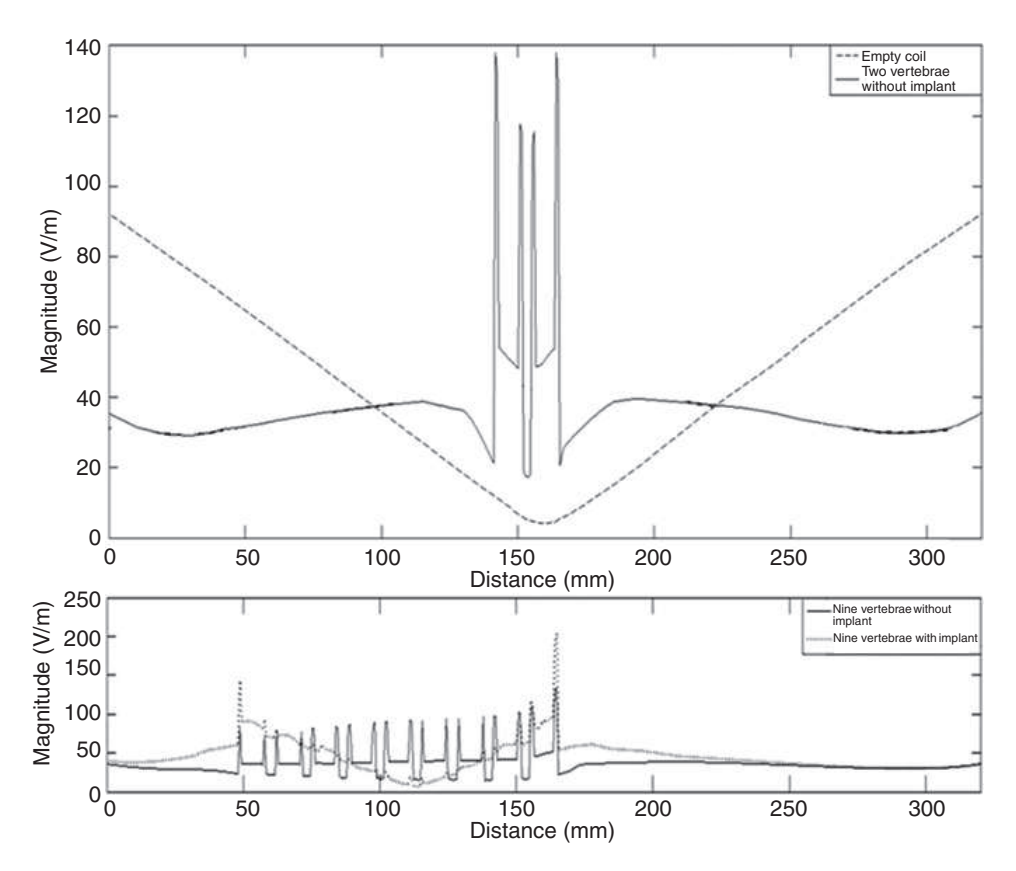


Figure 3: Medial layer of electrical fields examined in direction of the coil axis. Top: Dashed line indicates electrical field in empty coil and black line in two vertebrae model. Scale of amplitude [0, 140] V/m and distance [0, 325] mm. Bottom: Black line indicates electrical field in nine vertebrae model and dashed line in nine vertebrae spondylodesis model. Scale of amplitude [0, 250] V/m and distance [0, 325] mm.

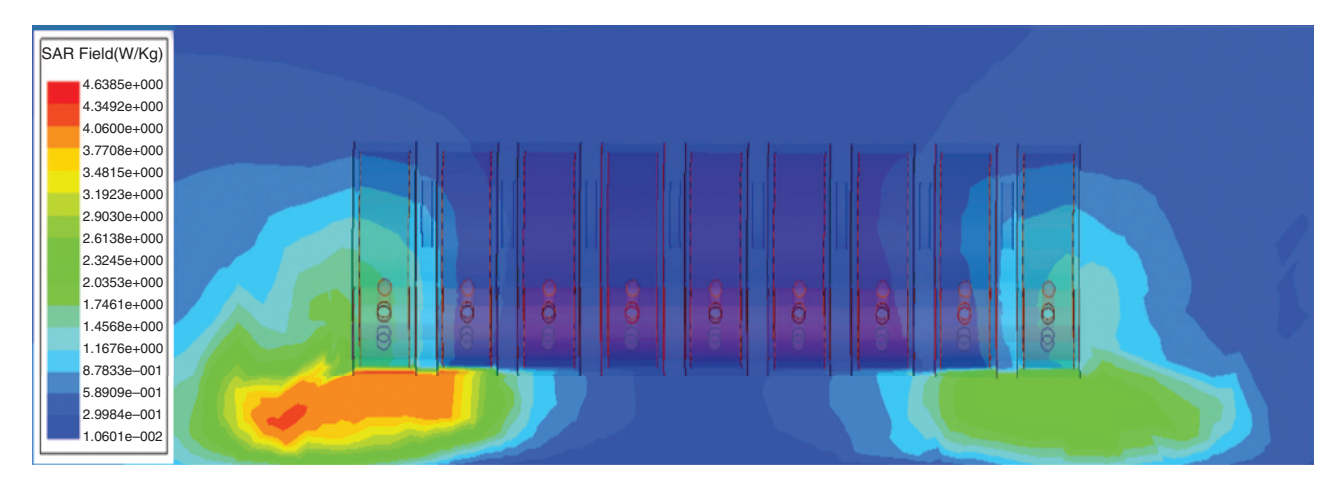


Figure 4: SAR in medial implant layer in 1.5 T MRI. SAR hotspots at rod edges spread posterior between implants and MRI table. SAR [0.01, 4.6] W/kg.

spondylodesis model consists of six or twenty titanium rods. Two rods along multi-vertebrae as frame rods with length $l_2=23.3$ mm, $l_9=116.4$ mm and diameter d=2 mm and four or eighteen rods with tip orthogonal to the frame rods as screws with length l=13.33 mm and diameter d=1 mm.

3 Results

The electromagnetic fields are examined in direction of the coil axis. In the empty coil the electrical field decreases linear to its minimum at the center and then increases

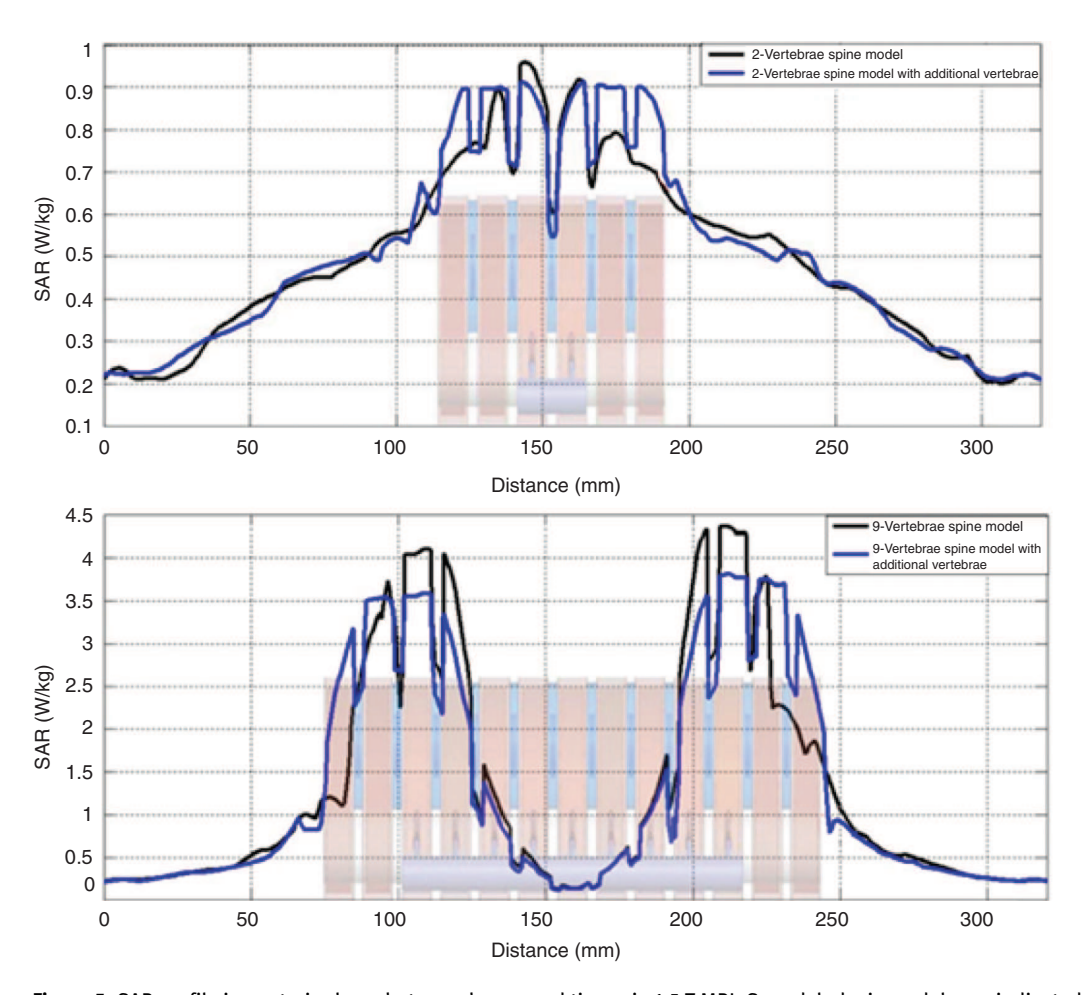


Figure 5: SAR profile in posterior layer between bones and tissue in 1.5 T MRI. Spondylodesis models are indicated as black line and models with additional vertebrae as blue line. Spondylodesis models with additional vertebrae are shown as an overlay to indicate the position for SAR variations. Top plot: models of small implant over two vertebrae. Scale of SAR [0, 1] W/kg and distance [0,325] mm. Bottom plot: models of large implant over nine vertebrae. Scale of SAR [0, 4.5] W/kg and distance [0, 325] mm.

with same gradient value. In vertebrae models along the coil axis the electrical field shows the posterior shape of vertebrae and spinal discs with high values at vertebrae and low values at spinal discs. In spondylodesis models this structure is still visible but with decreasing trend from distal to the model center and increasing to proximal (Figure 3).

The SAR is examined in direction of the posterior sagittal spine layer between bones and tissue (Figure 2). Along the implant SAR hotspots appear near the titanium rod edges and spread posterior between implants and MRI table (Figure 4). Between bones and tissue the SAR describes positions of vertebrae and disci intervertebrales. Maximum values are detected at vertebrae and minimum values at disci intervertebrales. Towards the model center values decrease (Figures 4–6). The SAR profile in spondylodesis models with additional vertebrae shows hotspots at vertebrae positions near rod edges with a slight decrease to the outer vertebrae, indicated as blue lines in Figure 5.

Compared to the spondylodesis model without additional vertebrae in Figure 6 the maximum intensity is lower.

4 Discussion and conclusion

SAR values in 1.5 T MRI are up to 600% higher with implant models than without [12]. Values in Table 2 distinguish the large scale variations due to the impact of implant size. In the spondylodesis model over nine vertebrae in 1.5 T SAR varies about 840% and in 3 T about 255%. The multiplyer of SAR in spondylodesis models over two vertebrae between 1.5 T and 3 T is five.

The results shown in Figures 5 and 6 approve the global pattern that energy deposition is related to the implant size [2]. SAR hotspots appear at implant edges and with sufficient rod length, here over nine vertebrae, extinction to the model center occures (Figures 4–6). Figure 3

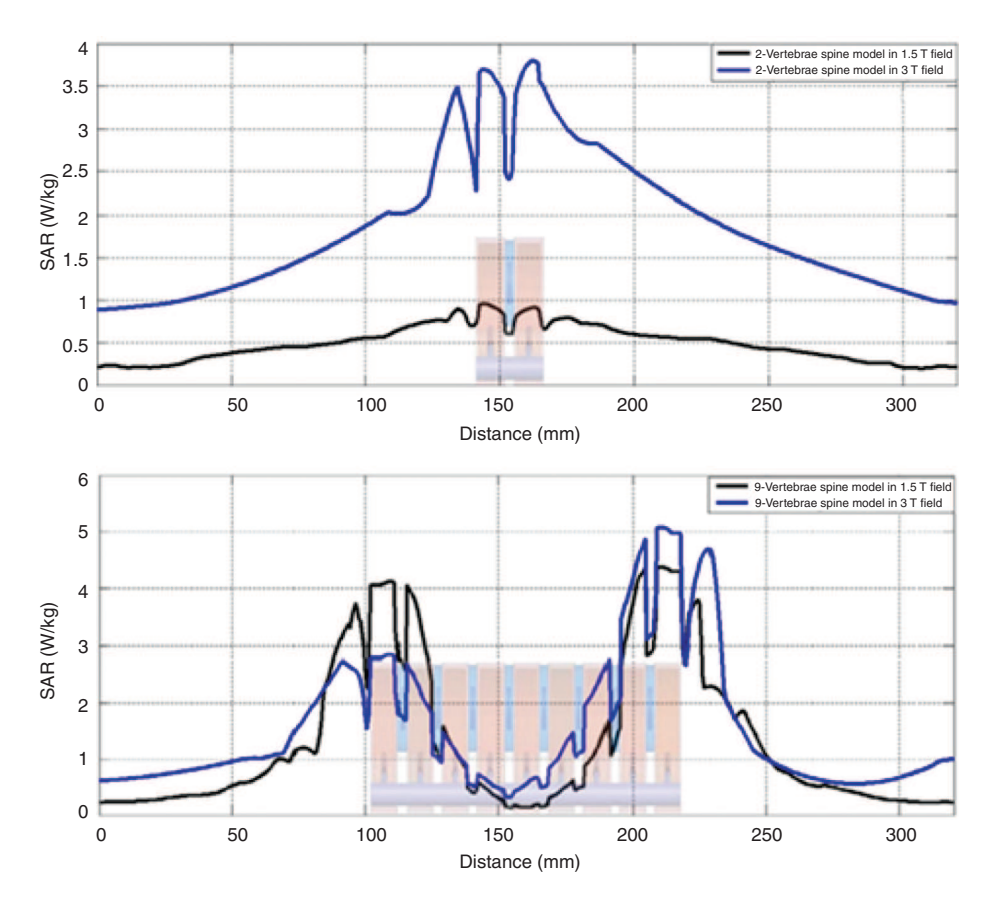


Figure 6: SAR profile in posterior layer between bones and tissue in spondylodesis models in 1.5 T MRI indicated as black line and 3 T MRI as blue line. Spondylodesis models are shown as an overlay to indicate the position for SAR variations. Top plot: models of small implant over two vertebrae. Scale of SAR [0, 4] W/kg and distance [0, 325] mm. Bottom plot: models of large implant over nine vertebrae. Scale of SAR [0, 6] W/kg and distance [0, 325] mm.

Table 2: SAR Hotspots near titanium rod edges at distal vertebrae, proximal vertebrae and extinction in model centers. All values are in [W/kg].

Layer	Model	SAR_{dis}	SAR_{prox}	SAR _{min}
	1.5 T MRI			
Between bones	2 vertebrae	0.68	0.69	0.2
and tissue	9 vertebrae	2.55	4.2	0.05
	2 additional v	ertebrae at	implant edges	S
Between bones	2 vertebrae	0.9	0.905	0.55
and tissue	9 vertebrae	3.55	3.8	0.1
	3 T MRI			
Between bones	2 vertebrae	3.6	3.8	2.45
and tissue	9 vertebrae	2.9	5.1	0.2

compared to Figures 5 and 6 show that extinction in SAR relates to electrical field profile in spondylodesis models. Further more the results lead to conclusion that energy absorption depends on bone and tissue geometry, since

the SAR profile between bones and tissue describes positions of vertebrae and disci intervertebrales with high values at vertebrae and low values at disci intervertebrales similar to the electrical field profile. Due to the fact that bone influences electrical fields the spine model needs to be enhanced.

Author's Statement

Research funding: The author state no funding involved. Conflict of interest: Authors state no conflict of interest. Material and Methods: Informed consent: Informed consent is not applicable. Ethical approval: The conducted research is not related to either human or animals use.

References

[1] Liu Y, Chen Y, Shellock F, Kainz W. Computational and experimental studies of an orthopedic implant: MRI-related heating at 1.5-T/64-MHz and 3-T/128-MHz. J Magn Reson Imaging. 2013;37:491-7.

- [2] Liu Y, Shen J, Kainz W, Qian S, Wu W, Chen J. Numerical investigations of MRI RF field induced heating for external fixation devices. Biomed Eng Online. 2013;12:12.
- [3] Frese G. Vorschriften und Normen zur MR Sicherheit. Siemens Medical Solutions; 2004.
- [4] Nitz WR. Praxiskurs MRT. Georg Thieme Verlag; 2011.
- [5] National Institute of Health. Available at: http://www.ncbi.nlm.nih.gov/pmc/articles/PMC3729307/ (Accessed: 20.04.2016).
- [6] Stenschke J, Li D, Thomann M, Schaefers G, Zylka W. A numerical investigation of RF heating effects on implants during MRI compared to experimental measurements. Springer Proceedings in Physics. Advances in Medical Engineering, Springer; 2007. p. 53-58.
- [7] Smajic-Peimann S, Zylka W. Simulation of SAR and temperature distributions for human organs with two different

- Birdcage designs at 42,6MHz and 127,8MHz. Biomed Tech. 2010;55.
- [8] ANSYS HFSS, Online Help, ANSYS; 2014.
- [9] International Electrotechnical Commission. Available at: https://webstore.iec.ch/preview/info_iec60601-2-33%7Bed3.1%7Db.pdf (Accessed: 20.04.2016).
- [10] Gabriel C, Gabriel S, Corthout E. The dielectric properties of biological tissues: I. Literature survey. Phys Med Biol. 1996;41 :2231-49.
- [11] Gabriel S, Lau RW, Gabriel C. The dielectric properties of biological tissues: III. Parametric models for the dielectric spectrum of tissues. Phys Med Biol. 1996;41:2271-93.
- [12] Hadert N, Zylka W. Numerical examinations of energy absorption in simplified spondylodesis models. YRA -Young Researchers Academy MedTech in NRW; 2016. DOI: 10.17185/duepublico/40821.